The Journal of Energy: Engineering & Management
Vol. 12, No. 4, Winter 2023, P. 80-99
Research Article

Economic, Exergy, and Environmental Analyses of Parabolic Trough Solar Collector with Turbulator Containing Polymer Hybrid Nanofluid

Ali Hosseini esfahani[1], Mehdi Aliehyaei[2*], Ali Hassani Joshaghani[3], Mohammad Mahdi Najafizadeh[4]

[1] Department of Mechanical Engineering, Arak Branch, Islamic Azad University, Arak, Iran
alihosseinni.s@gmail.com
[2] Department of Mechanical Engineering, Pardis Branch, Islamic Azad University, Parids City, Iran
aliehyaei@yahoo.com
[3] Department of Chemical Engineering, Arak Branch, Islamic Azad University, Arak, Iran
a-hasani@iau-arak.ac.ir
[4] Department of Mechanical Engineering, Arak Branch, Islamic Azad University, Arak, Iran
m-najafizadeh@iau-arak.ac.ir

Received: 7/12/2022 **Accepted:** 1/02/2023

Abstract
The limited resources of fossil fuels and the problems caused by greenhouse gas emissions have made it increasingly necessary to pay more attention to renewable energy sources, especially solar energy. Increasing the efficiency of equipment related to this group of energies will increase productivity, decrease fuel costs and electricity, and improve air quality. This study aims to design a new geometry for turbulators which increase efficiency in solar collectors, especially in higher Reynolds number (*Re*), with an increase in the Nusselt number (*Nu*) and a decrease in the pressure drop *(ΔP*). In this regard, the performance evaluation criterion (*PEC*) has been defined based on *ΔP* and *Nu*, and its changes have been investigated. Furthermore, the heat-transfer characteristics and performance of water-based *CuO-SWCNT* hybrid nanofluids (*HNF*), with volume fractions (ϕ) of 2% to 6% of nanoparticles in the *Re* = 12000 to 18000, have been investigated in the absorber tube of a solar collector. In order to couple velocity and pressure equations, a simple algorithm is used. Results from the study of two samples of twisted tape (*TT*) with two different scales (1 and 0.5) are examined for samples A and B respectively. Based on the results, the *TT* with a scale has the highest efficiency of 1.0 (*Re* =12000, ϕ = 2% is 3.54) where it is 3.52, while considering a *TT* with a scale of 0.5 under the same conditions. Therefore, using a *TT* with a scale of 1 is more desirable from a thermal fluid dynamics point of view.

Keywords: Twisted-tape turbulator, parabolic trough solar collector, hybrid nanofluid, *PEC*, efficiency.

* Corresponding author
doi: 10.22052/JEEM.2023.113688

1. Introduction

Throughout human history, sunlight has been used for heating and lighting, but recently it has been used for other purposes such as cooling, detoxification, and water desalination. Easy and widespread access, cost-effectiveness, cleanliness, and renewability of this energy source, all, have resulted in an increase in the use of solar energy and in the construction of various solar power plants [1]. Among these linear parabolic power plants, there is Solana power plant in the USA in Arizona with a production of 280 *MW* and Solena power plant in Seville with 150 *MW*. Solar Power Plants have parabolic mirrors that reflect sunlight at their focal point. Tubes in the center of the mirrors contain heat transfer fluid which absorbs heat from the sun radiation. The main advantage of these power plants is the possibility of storing solar energy; this thermal energy allows the power plants to generate electricity during the night [2].

Today, to promote the use of solar power plants, researchers have tried to increase the efficiency of these power plants so that the installation of these power plants is economical due to their high initial cost [3]. There are two main groups of applications for *PTC*: a) electricity generation and b) thermal applications in industrial processes. An increase in energy demand requires an increase in energy efficiency and heat transfer system equipment. Due to high energy demand, solar energy, in the recent decades, has become widespread [4]. Concentrated solar power plants (*CSPs*) are among the leading renewable energy technologies for power generation using the Rankine cycle. The technology is commonly used for commercial projects with capacities between 10 and 90 *°C* and operating temperatures between 300 and 400 *°C* [5]. Recently, *CSP* projects have been improved due to the improved efficiency of solar-related equipment, and reduced costs have become widespread [5, 6]. It is noteworthy to mention that in the recent years cogeneration through centralized solar energy technology (*CSP*) along with organic Rankin cycle (*ORC*) with potential applications in industrial processes has been a new way of using solar energy [6].

The development of parabolic concentrators for industrial processes has recently been one of the objectives of solar thermal engineering. A number of previous research projects have dealt with the development of new devices, applications, control methods, thermodynamics, and technical-economic analysis. To increase the efficiency of solar collectors, it is important to produce a high convection heat transfer coefficient between the surface of the absorber and the thermal fluid. There are three types of heat transfer enhancement techniques: active, passive, and hybrid. In active techniques, increased heat transfer occurs due to external power. Passive techniques use geometric changes without external power [7]. By creating a circulating turbulence flow, modified twist tape is one of the passive techniques for increasing the rate of heat transfer and reducing pressure. Thermal performance can be improved by altering fluid flow inside a pipe using inserts in the tube [8, 9]. Passive methods, without any need for input energy, on rough surfaces [10, 11], corrugated tubes [12, 13], insert turbulator, and nanofluid additives [14-16] are concentrated.

Previous articles have extensively studied the use of *TT* in tubular heat exchangers as a passive method to increase heat transfer. The use of *TT* inserts has a more negligible effect on pressure drop (ΔP) than the other techniques [17-19]. *TT* enables a turbulent-like mixed-flow which increases heat transfer [20-22]. Therefore, this issue has led to widespread utilization of this insert inside the pipes [23-25]. In 1964, 1976, and 1993, Smithberg and Landis [26], Hong and Bergels [27], and Manglick and Bergels [28] investigated the heat transfer efficiency of a heat exchanger tube equipped with a conventional *TT*. Also, Klepper [29] showed that the utilization of *TT* had increased the heat transfer rate by about 2 or 3 times compared with an ordinary pipe; thus, the use of *TT* in heat exchanger applications is advantageous. Many devices have been tested with twisted strips to enhance heat transfer [30-33].

A number of changes have been made to twisted strips such as toothed torsion strips (*TPP*) [34], multiple *TT* [35], and self-twisting *TT* [36, 37]. Twisted strips can also play an essential role in improving the performance of solar water heating systems [38]; the inserts can be inserted into flow pipes in solar water heating systems to increase heat transfer. In spite of this, they may result in significant increases in pumping power and operating costs. Another approach is to use nanofluids as the working fluid. However, in most previous studies, water, as the working fluid in the absorber tube, was used. Nevertheless, the utilization of water-soluble fluids is finite in cold regions such as Norway, Canada, Russia, and Iceland where water freezes at its freezing point. Due to this, additives that reduce the freezing point and increase the boiling point of the operating fluid are commonly used in shallow operating temperatures [39, 40]. Other essential benefits of utilization of nanofluids in the *PTC* collector include increased exergy efficiency and energy and increased Nusselt. However, they have disadvantages such as increased ΔP and investment costs [41]. At high temperatures, nanofluids are more important in *PTC* [42]. Both Nu and ΔP increase simultaneously when these two methods are used at the same time. This can be accomplished by using helically *TT* with Al_2O_3/*Water* nanofluid as the operating fluid [43] or *TT* with rectangular sections and four types of nanofluid as operating fluids [44]. The type, size, shape, and volume of a nanoparticle are also essential parameters for increasing heat transfer [45]. Akyork et al. [46] used a coiled turbulator to study the turbulent heat transfer of nanofluids inside a concentric heat exchanger. ΔP changes were not significantly affected by nanofluids at lower nanoparticle volume fractions.

Hybrid nanofluids are expected to increase thermal conductivity evaluated to nanofluids due to their positive effects [47, 49]. There have been valuable studies in mathematical modeling and nanofluids [49-52]. Therefore, it is essential to select an appropriate ϕ to ensure that a better η is gained [53]. Based on the review of the above articles, it becomes clear that many numerical methods have been investigated to increment the performance of solar collectors through the adoption of corrections in the selection of the appropriate operating fluid and changes in the geometry of the twisted strip inside the absorber tube. However, no study has been performed on heat transfer characteristics and efficiency coefficients in a pipe equipped with twisted strip grades utilization hybrid nanofluid, *SWCNT-CuO-Water*, as the fluid as well as the use of tertiary composite nanoparticles (*THNPS*). Most previous experimental and numerical studies concentrated on single and binary nanofluids [54].

The present study has been done to modify the geometry of the *TT* to increase the efficiency of solar collectors. A study has been conducted on the geometric shape effects of *TT* degrees on efficiency, Nusselt number (*Nu*), and *PEC* thermal performance coefficient. Simulations have been accomplished in a turbulent flow for *Re* in the range 12000 to 18000, under constant heat flux (1200 W/m^2). Therefore, the simulation and investigation of the effect of *Nu*, *PEC*, and η terms on the twisted strip model with different step ratios concerning hybrid nanofluid, as the working fluid, are the innovations of this study. In other words, the innovations of this study are:

- The numerical simulation of the Parabolic Trough Solar Collector, equipped with this model of the geometric shape of the turbulator, has not attained the attention of researchers.
- Until now, the environmental and economic analysis of *SWCNT-CuO-water* hybrid nanofluid in Parabolic Trough Solar Collector has not been investigated by any researcher.
- The simultaneous investigation of hydraulic-thermal analysis, exergy efficiency, and energy efficiency in the Parabolic Trough Solar Collector equipped with this model of the geometric shape of the turbulator has not been investigated by any researcher.
- The effect of using this turbulator geometric model on environmental and economic analyses in Parabolic Trough Solar Collectors has not been investigated by any researcher.

2. Description of the Physical Model

Fig.1 illustrates a general schematic of the proposed system. The combination of a tube with a *TT*, shown in samples A and B, has been investigated. *CuO-SWCNT-Water* hybrid Nano-fluid enters the absorbent tube with different ϕ values of 2%, 4%, and 6% at different velocities at 300 *K*. At the same time, a constant heat flux equal to 1200 W/m^2 does so. The parameters of the simulated model are fully shown in Table 1.

3. Boundary Conditions and Dimensionless Parameters

As seen in the image above, a three-dimensional channel model with *TT* is considered a computational field. At the fluid outlet, a zero relative pressure is used, and the inlet temperature is 300 *K* without any slip boundary conditions. The channel wall is exposed to 1200W/m^2 heat flux. The purpose of this study was to evaluate the results of the thermal and hydraulic performance numerically through using the definition of parameters such as *Nu*, Performance Evaluation Criteria (*PEC*), coefficient of friction (*f*), and the Reynolds number (*Re*).

The local convective heat transfer coefficient is as follows [55]:

$$h_x = \frac{q''}{T_w - T_b} \tag{1}$$

where "T_w" and "T_b" show the temperature of the inner surface and the temperature of the operating fluid.

The local *Nu* [55, 56]:

$$Nu_x = \frac{h_x D_h}{k_f} \tag{2}$$

$$D_h = \frac{4\,A}{P} \tag{3}$$

The *Re* is as follows [55, 56]:

$$Re = \frac{\rho \mathrm{U} D_h}{\mu} \tag{4}$$

The coefficient of friction (*f*) is defined as [55, 56]:

$$f = 2\Delta P D_h / \rho u^2 L \tag{5}$$

Prandtl number (*Pr*) [55, 56]:

$$Pr = \frac{\mu C_p}{k} \tag{6}$$

A performance evaluation criteria (*PEC*) is defined as [55, 56]:

$$(\dot{V}\Delta P)_s = (\dot{V}\Delta P)_{TT} \tag{7}$$

$$(fRe^3)_s = (fRe^3)_{TT} \tag{8}$$

$$Re_s = Re_{TT}(f_{TT}/f_s)^{1/3} \tag{9}$$

$$PEC = \frac{h_{TT}}{h_s}|pp = \frac{Nu_{TT}}{Nu_s}|pp = \left(\frac{Nu_{TT}}{Nu_s}\right)\left(\frac{f_{TT}}{f_s}\right)^{-1/3} \tag{10}$$

4. Governing Equations

The governing equations of the problem have been modeled using ANSYS 19.2 software, which is based on the finite volume method (*FVM*) [57]. *CuO* nanoparticles and *SWCNT* have been simulated using a single-phase method. The inlet and outlet areas ($L/3$) are considered respectively to ensure the development of the inlet flow and the impossibility of its return. In addition to simplicity, this method has good accuracy for simulation, so it has been used in most articles. The equations of conservation of mass (assuming constant nanofluid flow, incompressible and constant thermophysical properties, and negligible viscosity loss), conservation of momentum, and conservation of energy are defined as follows: [58]:

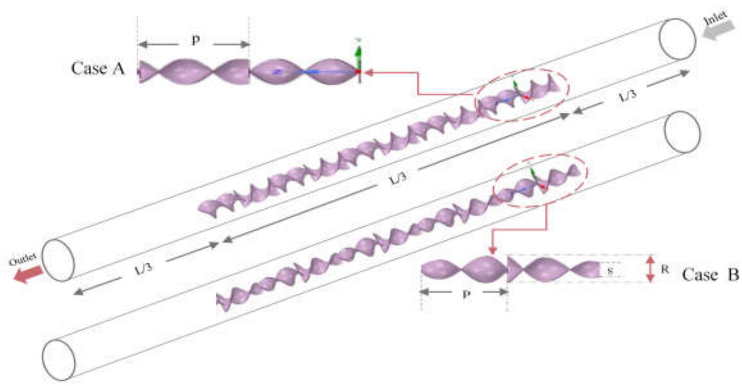

Fig. 1: Modeled geometry

Table 1. Specifications of the simulated model of the tube

Tube's specifications	$L = 600\ mm$	$D = 18\ mm$	-
Twisted tape turbulator specifications	$P = 20\ mm$	$S = 5\ mm$	$R = 10\ mm$

$$\frac{\partial u}{\partial x} + \frac{\partial v}{\partial y} + \frac{\partial w}{\partial z} = 0 \tag{11}$$

$$\rho\left(u\frac{\partial u}{\partial x} + v\frac{\partial u}{\partial x} + w\frac{\partial u}{\partial x}\right) = -\frac{\partial p}{\partial x} + \mu\left(\frac{\partial^2 u}{\partial x^2} + \frac{\partial^2 u}{\partial y^2} + \frac{\partial^2 u}{\partial z^2}\right) \tag{12}$$

$$\rho\left(u\frac{\partial v}{\partial y} + v\frac{\partial v}{\partial y} + w\frac{\partial v}{\partial y}\right) = -\frac{\partial p}{\partial y} + \mu\left(\frac{\partial^2 v}{\partial x^2} + \frac{\partial^2 v}{\partial y^2} + \frac{\partial^2 v}{\partial z^2}\right) \tag{13}$$

$$\rho\left(u\frac{\partial w}{\partial x} + v\frac{\partial w}{\partial x} + w\frac{\partial w}{\partial x}\right) = -\frac{\partial p}{\partial w} + \mu\left(\frac{\partial^2 w}{\partial x^2} + \frac{\partial^2 w}{\partial y^2} + \frac{\partial^2 w}{\partial z^2}\right) \tag{14}$$

$$\left[u\frac{\partial T}{\partial x} + v\frac{\partial T}{\partial x} + w\frac{\partial T}{\partial x}\right] = \alpha\left[\frac{\partial^2 T}{\partial x^2} + \frac{\partial^2 T}{\partial y^2} + \frac{\partial^2 T}{\partial z^2}\right] \tag{15}$$

The symbols ε and K represent the perturbed dissipation and turbulent kinetic energies, respectively.

$$\frac{\partial}{\partial x_j}(u_j\varepsilon\rho) + C_{2\,\rho}\frac{\varepsilon^2}{k + \sqrt{v\varepsilon}} = \frac{\partial}{\partial x_j}\left[\left(\mu + \frac{\mu_t}{\sigma_\varepsilon}\right)\frac{\partial\varepsilon}{\partial x_j}\right] + \varepsilon S C_{1\,\rho} + C_{3\,\varepsilon}C_{1\,\varepsilon}\frac{\varepsilon}{k}G_b \tag{16}$$

$$\lambda = S\frac{k}{\varepsilon}, C_1 = max\left(\frac{\lambda}{\lambda + 5}.0.43\right)$$

$$\sigma_k = 1\ ,\ C_{1\,\varepsilon} = 1.44, C_2 = 1.9\ ,\sigma_\varepsilon = 1.2$$

$$\rho\frac{\partial}{\partial x_j}(Ku_j) = G_k + \frac{\partial}{\partial x_j}\left[\frac{\partial K}{\partial x_j}((\sigma_k)^{-1}\mu_t + \mu)\right] + G_b - \varepsilon\rho \tag{17}$$

The *k-ε* Realizable turbulence model is another K-Epsilon turbulence model subset.

$$G_k = -\rho\overline{u_i'u_j'}\frac{\partial u_j}{\partial x_i}, G_b = \beta g_i\frac{\mu_t}{Pr_t}\frac{\partial T}{\partial x_i}\ , Pr_t = 0.9 \tag{18}$$

$$S_{ij} = \frac{1}{2}\left(\frac{\partial u_j}{\partial x_i} + \frac{\partial u_i}{\partial x_j}\right), S = \left(2S_{ij}S_{ij}\right)^{0.5} \tag{19}$$

Also, the *k-ε* Realizable turbulence model works better than other models in the *k-ε* family when the flow has an inverse gradient or separation. Also, compared to the turbulence model, the RNG uses the *k-ε* model realizable and can lead to better stability [58]. The height of the first cell of the boundary layer depends on factors such as viscosity, the length of the viscous region, fluid velocity, density, and, most importantly the *Y+* value. Enhancing wall treatment was used in this study. Therefore, in this case, *Y+*<5 should be considered [58].

5. Solar Collector Equation

Fig.2 shows the general schematic of the *PTC* used in the present study, in which, given the specificity of the inlet and outlet temperatures of the solar collector, Eq. (19) has been used to calculate the efficiency. Solar radiation passes through the glass cover to reach the receiver (absorber tube). A portion of the heat absorbed is transferred to the operating fluid (useful energy), and the remainder is wasted.

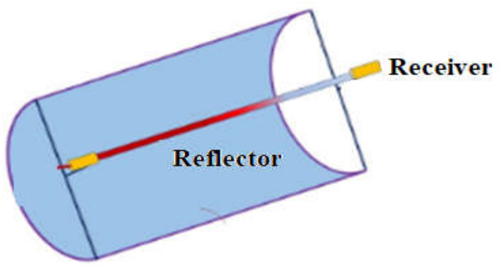

Fig. 2: Views of the solar collector

The energy efficiency of the *PTC* is calculated by [59, 60]:

$$\eta = \frac{Q_u}{Q_T} \tag{20}$$

A solar collector's thermal efficiency can be calculated using the following equation [59, 60]:

$$\eta_{th} = \frac{Q_u}{Q_s} \tag{21}$$

$$Q_u = \dot{m} C_p (T_o - T_{in}) \tag{22}$$

6. Hybrid Nanofluids Relations

The term hybrid nanofluid refers to those nanofluids that are composed of two or more nanoparticles [61]. A number of critical challenges have been identified for hybrid nanofluids including stability, pumping power, production costs, and the selection of appropriate volume fractions [62]. Heat capacity, density, dynamic viscosity, and thermal conductivity of *SWCNT-CuO-Water* hybrid nanofluid are defined as follows:

$$\rho_{hnf} = (1 - \phi_1 - \phi_2)\rho_{bf} + \phi_1 \rho_{np1} + \phi_2 \rho_{np2} \tag{23}$$

$$(\rho c_p)_{hnf} = (1 - \phi_1 - \phi_2)(\rho c_p)_{bf} + \phi_1 (\rho c_p)_{np1} + \phi_2 (\rho c_p)_{np2} \tag{24}$$

$$\mu_{hnf} = \frac{\mu_{bf}}{(1 - \phi_1 - \phi_2)^{2.5}} \tag{25}$$

$$k_{hnf} = k_{bf} \left(\frac{(k_{np1} + k_{np2}) + 2k_{bf} - 2\phi_{np1}(k_{bf} - k_{np1}) - 2\phi_{np2}(k_{bf} - k_{np2})}{(k_{np1} + k_{np2}) + 2k_{bf} + \phi_{np1}(k_{bf} - k_{np1}) + \phi_{np2}(k_{bf} - k_{np2})} \right) \tag{26}$$

Table 2 shows the properties of *water-CuO-SWCNT* hybrid nanofluid.

Table 2: Properties of *water-CuO-SWCNT* hybrid nanofluid

	$\rho(kg/m^3)$	$C_p(J/kg.K)$	$\mu(kg/(m.s)$	$k(w/m.K)$
CuO	6400	531.02	-	33
Swcnt	1600	730	-	3180
ϕ = 2%	1027.03	4037.51	0.000873	0.622234
ϕ = 4%	1057.06	3905.002	0.00089	0.63156
ϕ = 6%	1117.12	3661.359	0.00094	0.6505
Water	997	4178	0.00085	0.613

7. Numerical Method

ANSYS FLUENT 2019 software has been used using the FVM and *k-ε* Realizable model to discretize equations according to Manter et al. [63]. The coupling algorithm is utilized for pressure-velocity coupling. In the coupling method, the equations of momentum and continuity are solved simultaneously and together, which will increase the speed of convergence. Convergence criteria are 10^{-6}.

7.1. Grid of Mesh

In order to check the grid independence test, the geometry of the parabolic solar collector along with the turbulator (Case A) has been obtained for different modes from the Number of Elements. In addition, the obtained values of the Nu_{avg} for the mode's Number of Elements are reported. Fig. 3 shows the results obtained from the Nu_{avg} in the Number of Elements. As seen, while the Number of Elements increases, the values obtained from the Nu_{avg} increase. This is while from 1529998 onwards, with an increase in the Number of Elements, the values of the Nu_{avg} do not show significant changes. Therefore, the number of elements of 1529798 is suitable as an optimal network. Fig.4 describes the meshed geometry of the turbulator. As seen, the meshing is considered to be reasonably dense.

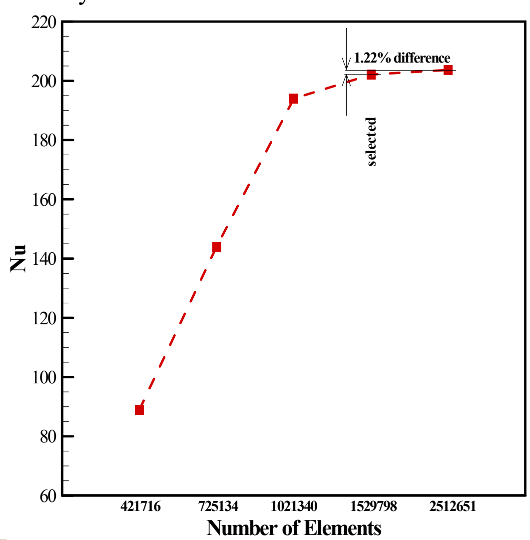

Fig. 3: Grid independence study for Case A turbulator for *Re* = 18000 and ϕ = 2%

7.2. Validation

The validation of the present work has been done by comparing the Nusselt numerical results (*Nu*) and the coefficient of friction (f) of the Dittus-Boelter and Blasius correlations respectively [84]; (Eqs.(26) and (27)) have been performed for simple tubes with simulated experimental results. Figs5 and 6 show the validation in the present study. The maximum deviations for *Nu* and coefficient of friction are about 6% and 5%. According to the numerical results, the *Nu* and friction coefficient are correlated with the standard experimental correlations. Therefore, the numerical model is considered reliable in the present study [64]:

$$Nu = 0.023Re^{0.8}Pr^{0.4} \quad \text{Dittus-Boelter} \quad (27)$$
$$f = 0.079Re^{-0.25} \quad \text{Blasius} \quad (28)$$

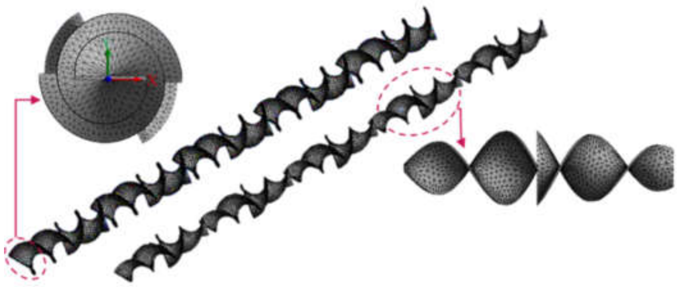

Fig. 4: Mesh of Simulated model

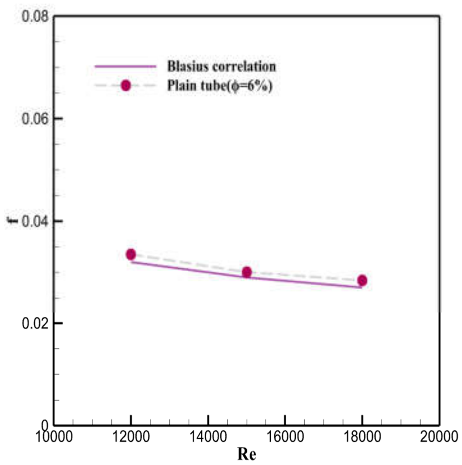

Fig. 5: Validation of friction coefficient values in terms of Reynolds in the present study with experimental results

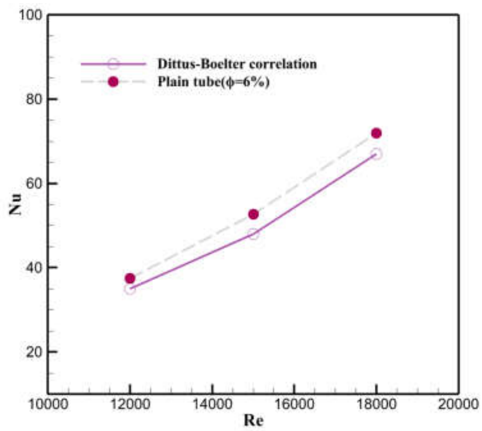

Fig. 6: Validation of Nusselt values in terms of Reynolds in the present study with experimental results

In addition, validation with experimental results has been done to ensure the solution method. Akyurek et al. [46] experimentally investigated the effect of using wire coils in a heat exchanger. Their study was done in the turbulent flow regime and the *Re* = 4000 to 20000. In addition, Al_2O_3*-water NF* in a ϕ of 0.4 to 1.6% was used as the working fluid in the study. In order to ensure the solution method, the values obtained from the Nu_{ave} in Akyürek et al. [46]. In the present study, these results were compared with those obtained from numerical simulations. In the present study, numerical simulation is based on the geometry and boundary conditions from Akyürek et al. [46]. In addition, numerical simulation has been performed for *Re* = 4000 to 20000 and ϕ = 1.6%. Fig. 7 shows the results obtained from the Nu_{ave} in the simulation of the present study with the results of Akyürek et al. [46]. As seen, the experimental and numerical results confirm each other with acceptable accuracy. *Also,* the maximum difference between experimental and numerical data is 2.96%.

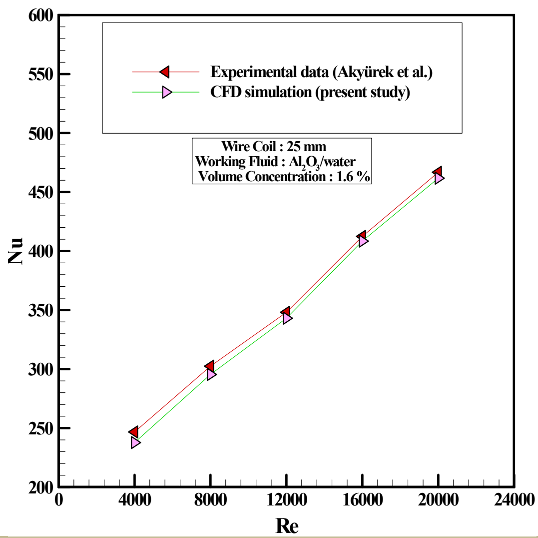

Fig. 7: Validation with experimental data [39]

8. Results and Discussion

8.1. Contours Related to Parabolic Trough Solar Collector with Turbulator

Fig.8 shows the velocity contour of samples A and B at *Re* = 12000 and ϕ = 0.02. By comparing the cut profiles of both samples at a distance of Z = 200*mm*, it becomes possible to observe a better and more uniform mixing of the flow velocity in sample A than in the other one. *Also,* according to the results inferred from Fig.9, the amount of radial velocity in the tube case with the presence of sample A, as a flow turbulator, is higher than sample B. A stronger centrifugal force, a more efficient interruption of the thermal boundary layer, rotational motion, and axial flow can all contribute to this. Higher Reynolds numbers lead to better flow mixing between the central and near areas of the wall at higher speeds which results in more efficient heat dissipation and more uniform temperature distribution. The turbulator also increases the velocity of the rotational flow, especially in areas where it is located. According to Fig.10, pipes equipped with turbulators (samples A and B) dissipate energy well from the wall of the tube to the center of the tube. This is also due to the greater mixing of fluids due to a turbulator, so better energy dissipation can lead to an increased heat transfer rate. The contour of the Turbulence Kinetic Energy change with increasing Reynolds number in a tube with sample-A is shown in Fig.11. The energy dissipation by the turbulator of sample A is better than that of sample B. An increase in flow velocity (Reynolds increase) improves fluid mixing resulting in better energy dispersion and uniformity from the pipe wall to the center as shown in Figure 8. *Also,* sample A has a more uniform Eddy viscosity than sample B due to stronger rotational flow, which is shown for *Re* = 18000 and ϕ = 2% in Fig.12. *Also,* the flow velocity increases with increasing Reynolds (Fig.13), and the Eddy viscosity becomes more uniform; this uniformity is higher for sample A than for sample B.

Fig.14 shows the temperature contours of the turbulators of samples A and B. the temperature of the tubular body of sample A is more uniform than that of sample B. It is relative to the inlet temperature of the fluid (300 *K*), in the way that the maximum temperature of the turbulator (at a distance of 1 mm from the inlet of the pipe) is 300.014 *K* and 300.016 *K* for samples A and B respectively. Figs. 15 and 16 show the pressure contours of both samples.

According to the results obtained from these contours, the ΔP of sample A decreases with an increase in intensity of rotational flow due to decreasing fluid contact surface and tube wall compared to sample B, which has better uniformity. This ensures that there is a pressure difference between the center of the tube and the turbulator (Z = 200-400 *mm*); for sample A, it is approximately 1.5 *kPa*, and for sample B it is equal to 1.6 *kPa*.

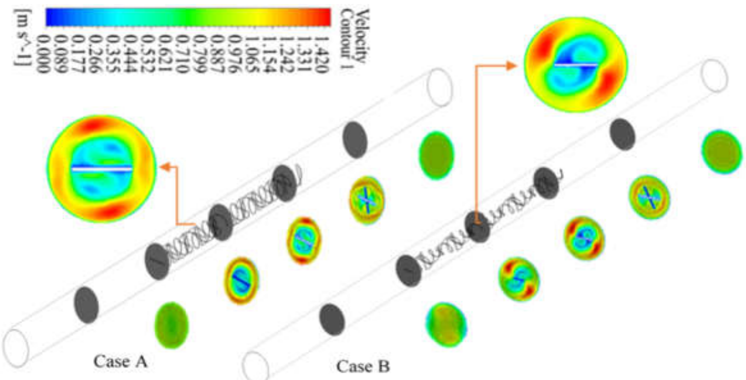

Fig. 8: Velocity contours of samples, A, B

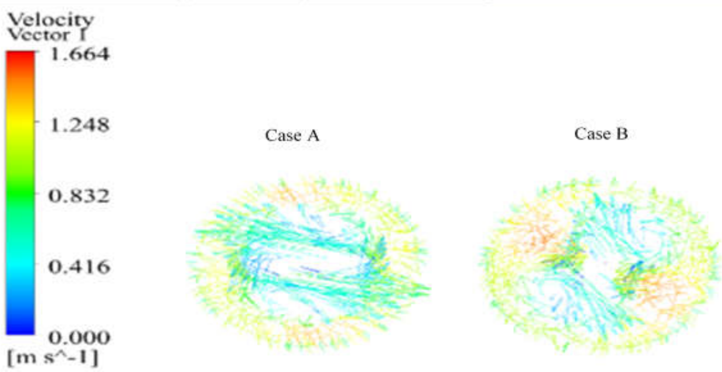

Fig. 9: Contour velocity vectors of samples A and B at distance *Z*

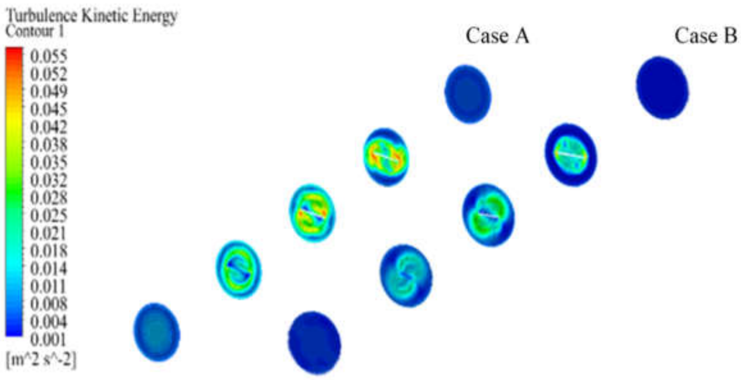

Fig. 10: Samples A and B of turbulence kinetic energy

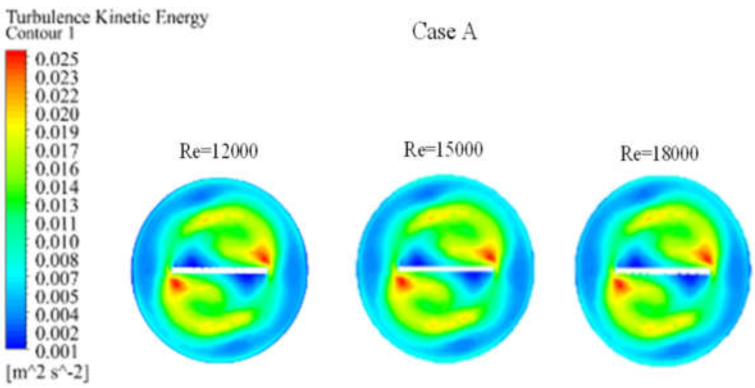

Fig. 11: Turbulence kinetic energy of sample A at distance *Z* = 300 *mm*

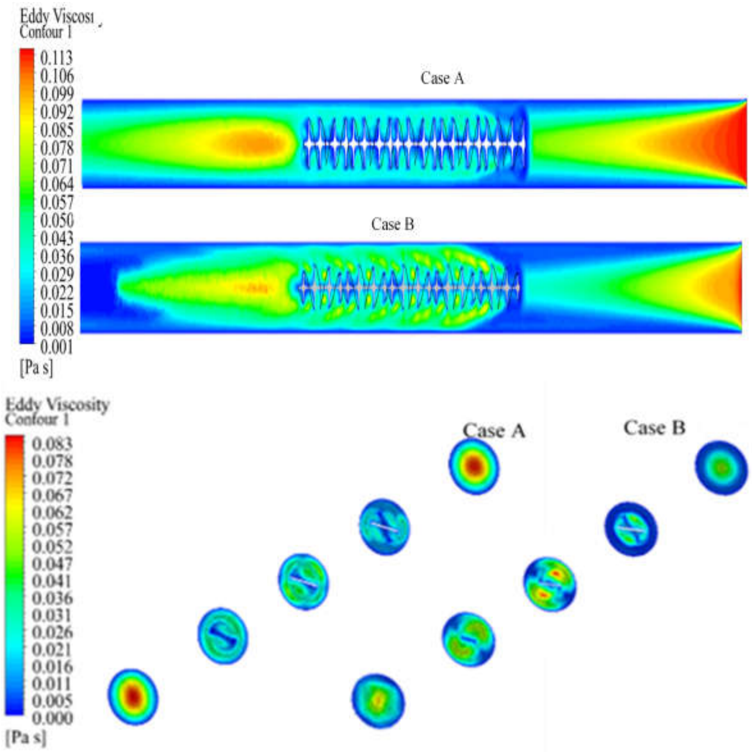

Fig. 12: Eddy viscosity contours for samples A and B

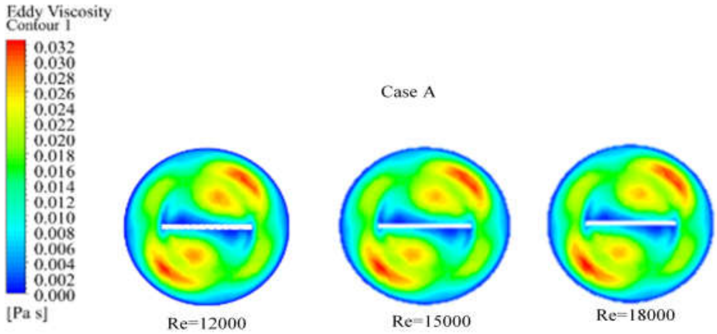

Fig. 13: Eddy viscosity contours of sample A at distance Z = 300 *mm*

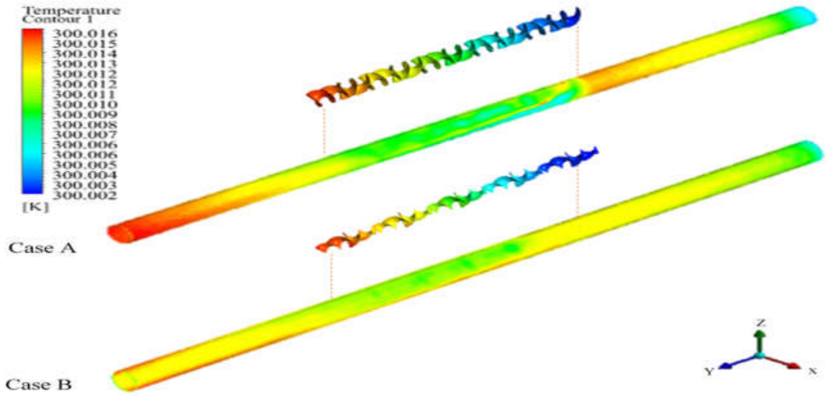

Fig. 14: Samples A and B temperature contour

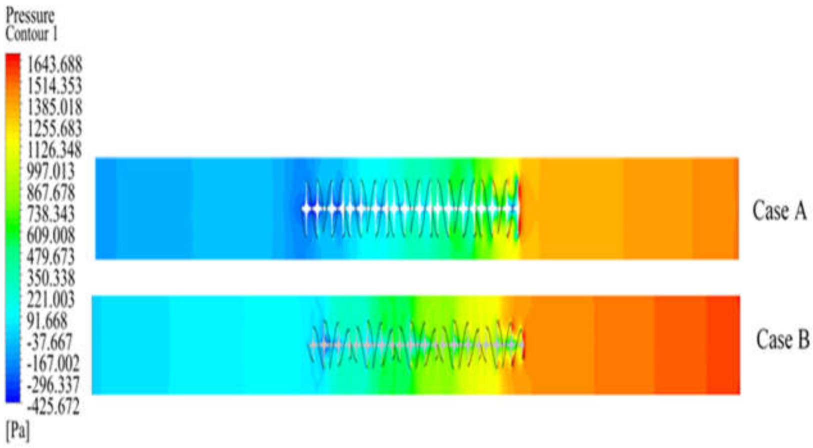

Fig. 15: Sample A pressure contour

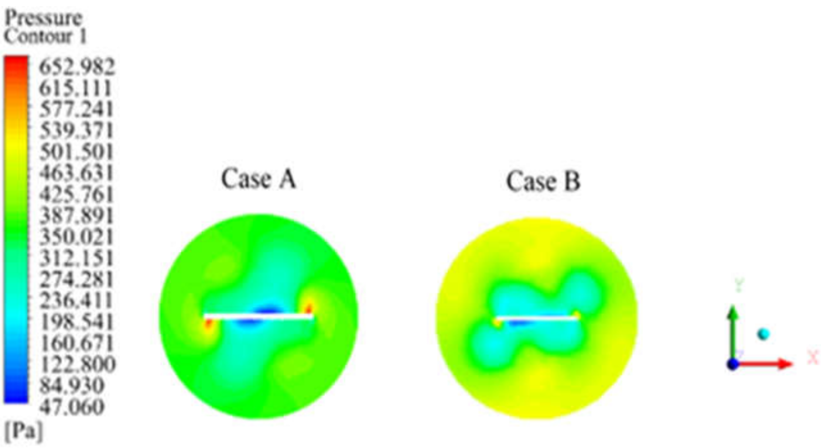

Fig. 16: Samples A and B pressure contour at a Z = 300*mm* distance

8.2. Changing *Nu* and *PEC* with Altering ϕ and *Re*

This study evaluates the thermal performance of twisted tape turbulators incorporated into a solar collector by numerical simulation. The significance of the twisted-tape scale size, the Reynolds number range (*Re*), and the volume fraction of hybrid fluid nanoparticles (ϕ) in two samples (A, B) have been evaluated separately.

The diagram of the change of *Nu* with Reynolds number for twisted strip with different scales samples (A and B) is shown in Figs. 17 and 18; Fig.17 presents a better comparison of the results having been obtained from both samples. As evidenced by previous studies, the presence of a twisted-tape turbulator in a simple tube increased the amount of heat transfer and, consequently, the *Nu*, shown in Figs. 17 and 18. Also, with increasing Reynolds (increasing the flow velocity) and decreasing the particle volume fraction, the *Nu* increased, and, thus, the heat transfer rate increased. According to the results of Fig.19, the heat transfer rate in the presence of sample A was higher than sample B so that the maximum *Nu* could be achieved in *Re* = 18000 and ϕ = 2% for samples A and B, which were 195 and 192 respectively.

Adding nanoparticles to the base fluid increased the heat transfer rate, but it increased frictional resistance and ΔP as well. Turbulators cause more turbulence and, thus, more heat transfer and *Nu* values. In addition, it increased friction coefficient, and ΔP. *Nu* numbers tended to be associated with more Δp.

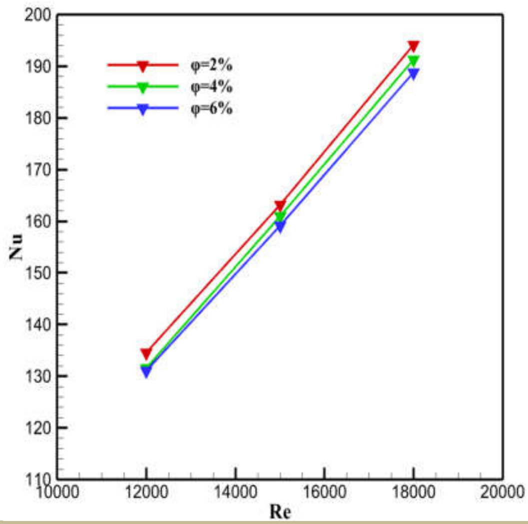

Fig. 17: Changes in the *Nu* in *Re* for sample A

In the present study, the *PEC* was introduced as a measurable criterion for evaluating the exchange between *Nu* and Δp. Through this criterion, the optimal point with the maximum thermal-hydraulic performance could be identified. For sample A, *PEC* coefficient decreased with increasing Reynolds and volumetric concentration of nanoparticles, as shown in Fig. 20.

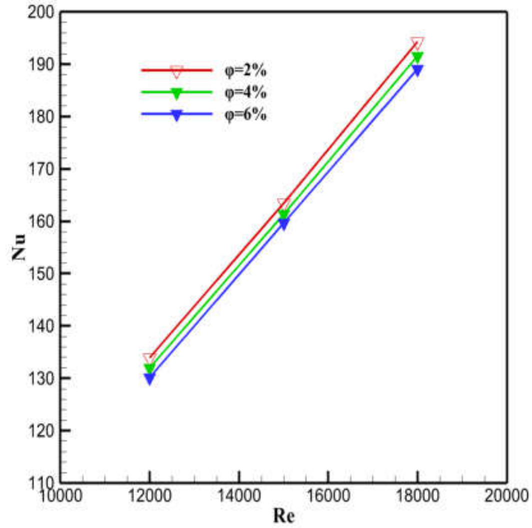

Fig. 18: Changes in the *Nu* in *Re* for sample B

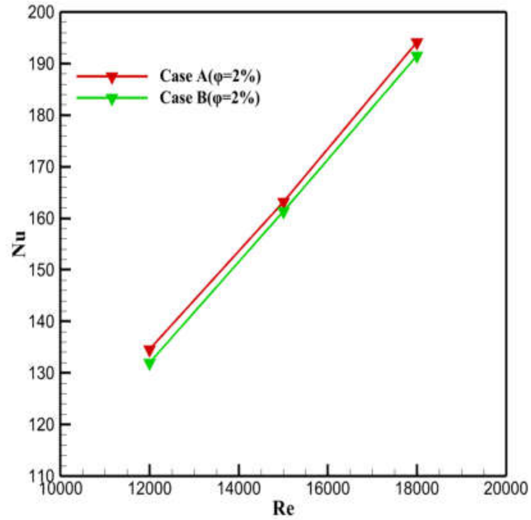

Fig. 19: Comparison of Nu_{avg} changes with Reynolds number for samples A and B

A comparison of the performance evaluation coefficient of samples A and B shown in Fig.21 shows that these two samples do not differ much in the values of the performance evaluation coefficient. However, sample A has higher values in the lower Reynolds numbers.

Therefore, using both samples is appropriate for the performance evaluation coefficient. Heat transfer always overcomes ΔP in both models in the range of Reynolds numbers and nanoparticle volume fraction investigated in this study. In fact, with an increase in Reynolds number and volume fraction of nanoparticles, the values of Nu_{avg} and ΔP increased. By increasing the inlet velocity, the mixture and turbulence of the hybrid nanofluid will be higher when it hits the turbulator. This is so, despite the fact that the ΔP caused by the heat transfer caused by the turbulator is acceptable.

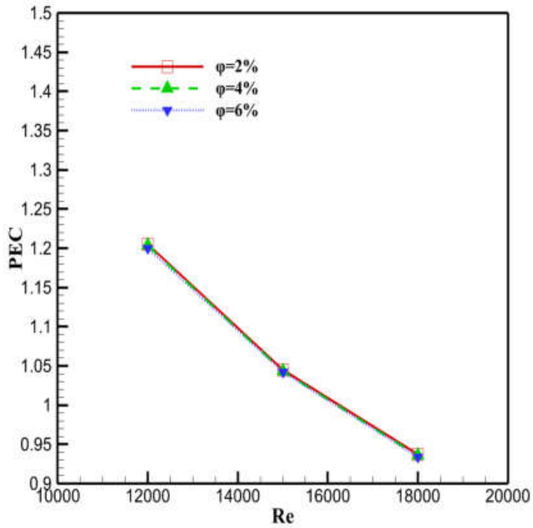

Fig. 20: Changes in Reynolds performance evaluation coefficient for sample A

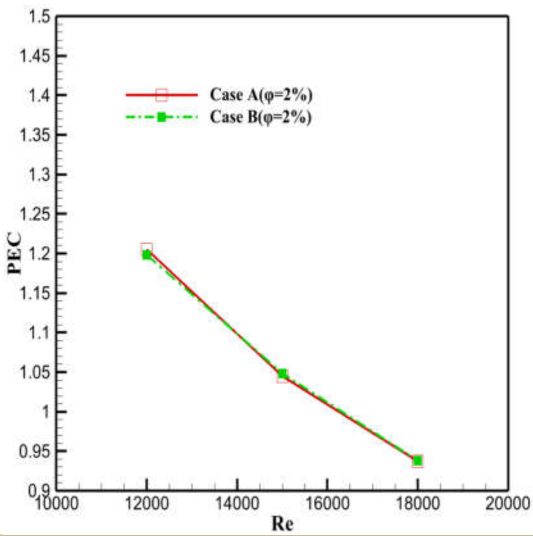

Fig. 21: Comparison of performance evaluation coefficient changes with Reynolds number for samples A and B

8.3. Solar Collector Efficiency Analysis

According to Figs. 22 and 23, samples A and B differ in energy efficiency based on Reynolds number and volume fraction of nanoparticles. Also, a comparison of the performance of samples A and B for a volume fraction of 2% is presented in Fig.24. In both samples, the efficiency of the solar collector decreases with incrementing *Re* and decreasing the ϕ. The changes in energy efficiency with volume fraction in sample A are more severe than those in the other sample. Thus, the energy efficiency at *Re* = 12000 decreases from 3.55 in ϕ = 2% to 3.44 in ϕ = 6% (about a 3.1 %decrease). Also, according to the results obtained from numerical simulation (Fig.22), the highest energy efficiency is related to sample A, with a maximum value of 3.55 at *Re* = 120000 and ϕ = 2%.

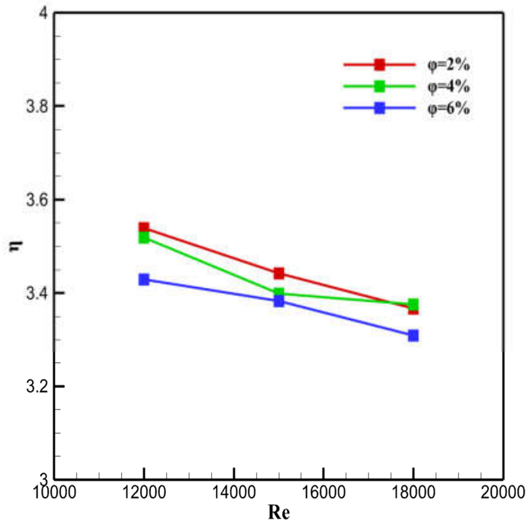

Fig. 22: Solar collector efficiency changes in Reynolds for sample A

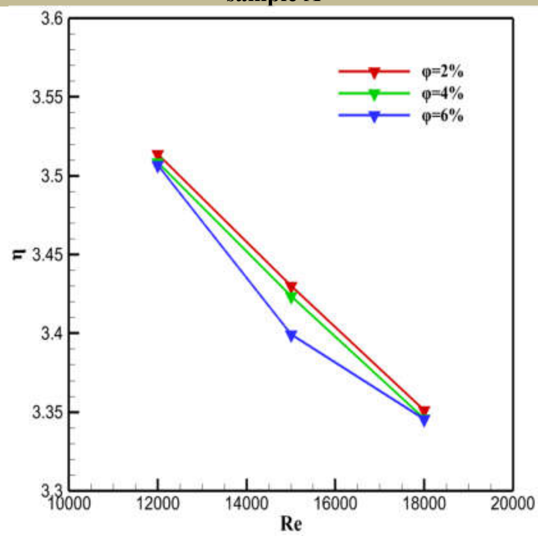

Fig. 23: Solar collector efficiency changes in Reynolds for sample B

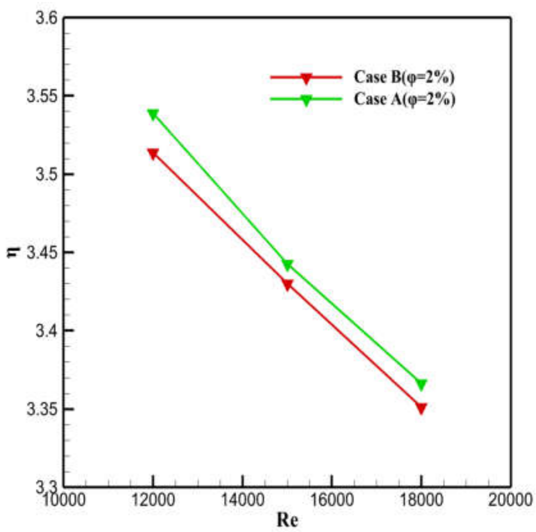

Fig. 24: Comparison of solar collector efficiency changes in Reynolds for samples A and B

8.4. Solar Collector Exergy Efficiency Analysis

High-temperature engineering equipment relies heavily on radiation heat transfer. Solar energy converters create a high limit for converting solar energy efficiency into work. According to the literature review, most of the accepted models based on solar radiation exergy are the Spanner, Petela, and Jeter models [65]. Jeter's approach deals with heat engine analysis, which describes heat radiation's exergy with Carnot efficiencies. According to Spanner, the exergy of direct solar radiation is related to precision rather than useful work [65]. Using the Petela model, based on thermal radiation at solar temperature, this study examines the exergy of solar radiation. Petla uses conservation equations to model the energy of emission flux of blackbody radiation. To model the energy of emission flux of blackbody radiation, Petla uses conservation equations [65]:

$$Ex_{rad.b} = \frac{ac}{12}(3\,T^4 + T_o^4 - 4T_oT^3) \tag{29}$$

In addition, Petela proposed the following equation for the gray surface with radiation [65]:

$$Ex_{rad.g} = \varepsilon\frac{ac}{12}(3\,T^4 + T_o^4 - 4T_oT^3) \tag{30}$$

Where a (a = 7.561×10^{-19} $KJ\ m^{-3}k^{-3}$) is the radiation constant, c (c = 2.998×10^{8} ms^{-1}) is the speed of light in a vacuum, and T is the absolute temperature. The ratio between the energy emitted by a surface and the energy emitted by a black body at the same temperature is called emission. This value is always between zero and one. This quantity shows how close the radiant properties of an actual surface are to a black body (the emission factor for a black body is one). As a result of the definition provided for this value, the following equation can be used to calculate this number [65]:

$$\varepsilon(T) = \frac{E(T)}{E_b(T)} = \frac{E(T)}{\sigma T^4}\ ,\sigma = 5.67 * 10^{-8}\frac{W}{m^2K^4} \tag{31}$$

The energy dissipation for an emitted surface is equal to:

$$E_{rad} = \varepsilon\frac{ac}{4}T^4 \tag{32}$$

Energy conversion efficiency (η_ε) can be expressed as the ratio of W to energy [65]:

$$\eta_e = \frac{W}{E_{rad}} \tag{33}$$

Petela exergy solar radiation equals maximum solar radiation efficiency according to the theory. Based on the maximum exergy of solar radiation to the maximum energy of solar radiation [65]:

$$\varepsilon = \eta_{e\,max} = \frac{Ex_{rad}}{E_{rad}} \tag{34}$$

Therefore, Petela efficiency can be defined as follows [65]:

$$\varepsilon = 1 + \frac{1}{3}\left(\frac{T_o}{T_s}\right)^4 - \frac{4}{3}\left(\frac{T_o}{T_s}\right) \tag{35}$$

The same formula is derived from Candau [66]. According to this researcher, the efficiency formula is always positive. If $T = T_{0,}$ the efficiency is 0; if $T < T_0$, the efficiency can be greater than 1. Spanner also proposed a different equation for maximum conversion efficiency. He introduced maximum economic efficiency (η_s) and assumed the radiation source to be a black body, so the specific exergy flux was shown below [66]:

$$\varepsilon_s = 1 - \frac{4}{3}\left(\frac{T_o}{T_s}\right) \tag{36}$$

Jeter theory is the work of the heat engine cycle, heat (q) is given to the engine at temperature (T), and this heat is converted to W work at Carno efficiency (η), which is equal to the efficiency of Jeter (η_j) conversion [66]:

$$\varepsilon_j = \eta_{Cs} = \frac{T_s - T_o}{T_s} = 1 - \frac{T_o}{T_s} = \frac{W_j}{q_j} \tag{37}$$

Figs. 25 and 26 illustrate the changes in exergy efficiency for samples A and B in terms of Reynolds number and nanoparticle volume fraction.

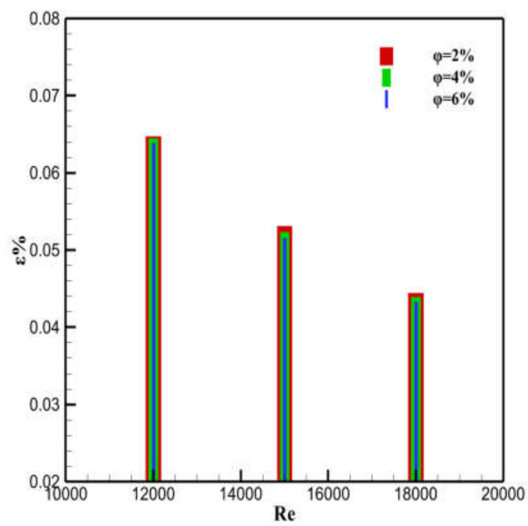

Fig. 25: Changes in exergy efficiency in terms of *Re* for sample A

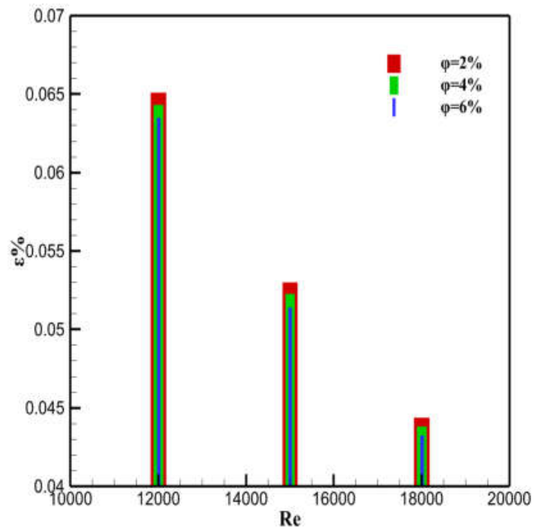

Fig. 26: Exergy efficiency changes in terms of *Re* for sample B

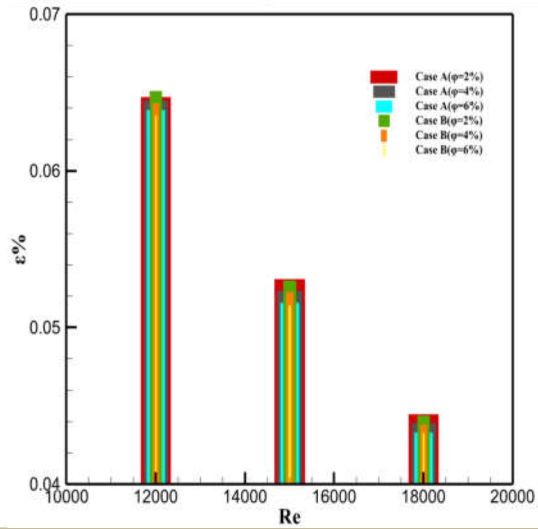

Fig. 27: Comparison of exergy efficiency changes for samples A and B

A comparison of the performance of samples A and B for a volume fraction of 2% is also presented in Fig.27. In both samples, with increasing Reynolds and volume fraction, the efficiency of the solar collector decreases so much so that the highest exhaust efficiency is obtained at ϕ = 2% and *Re* = 12000 for both samples. Also, according to the results obtained from the numerical simulation of Fig. 27, the highest exergy efficiency is related to sample A, with a maximum value of 0.0064 obtained in ϕ = 2% and *Re* = 12000. With increasing velocity, the exergy efficiency of the fluid containing nanoparticles decreases approximately for sample A.

8.5. Economic Analysis

A suitable method for the economic evaluation of solar systems is the Levelized cost of energy (*LCOE*) [67, 68]. In the present study, only the cost of the collector (*CO*) with the studied working fluid is considered; this costis 200 (*Euro/m^2*) for *PTC* with smooth-surfaced absorbent tube and 200(*Euro/m^2*) for *PTC* with hybrid turbulator absorbent tube which is about 3% more [69]. The *PTC* in question has an aperture of 85 *m^2*, so the cost of the collector with smooth-absorbent tubes and a combined turbulator is about 17,000 and 17,500 euros respectively. To calculate the *LCOE*, the following equation [70] was used:

$$LCOE = \frac{CO}{Q_u N} = \frac{CO}{\eta_{th} Q_s N} = \frac{CO}{\dot{m} C_p (T_o - T_{in}) * N} \tag{38}$$

Where *N* is the total operating hours of the system, this parameter is calculated for the entire lifetime of the operational *PTC*. Considering the average lifespan of mechanical equipment, the current study's *N* parameter is about 24000 hours (total life of 20 years, with 1200 hours per year). Figs. 28 and 29 show the change in *LCOE* with Reynolds number and nanoparticle volume fraction for samples A and B respectively. On the other hand, as the flow velocity and volume fraction of nanoparticles increase, the *LCOE* value decreases. The leading cause of *LCOE* changes is related to the thermal efficiency of the collector, which is the denominator of the equation.

8.6. Environmental Analysis

The investigation of the level of environmental pollutants in heat transfer systems is crucial. In the present study, to evaluate the number of pollutants including CO_2, NO_x and SO_x reducing the size of the collector diaphragm area and latent energy has been used [71-73]. Latent energy is the sum of the entire energy required to produce any product or service as if it were energy in the product included or "hidden". The latent energy can be calculated through the following equation [73]:

*Embodied energy= Volume of material*Density of material* (39)

Environmental pollutants in the collector life cycle are created by various fuels such as oil, coal, and natural gases. The life cycle of *PTCs* involves many stages, including manufacturing, distribution, maintenance, and disposal [74]. In this analysis, the amount of pollutants is calculated only in the collector construction stage. Several environmental pollutants are provided for different fuel sources [75]. Since the *PTC* is made of glass and steel, the latent energy for these components is based on their mass calculation. Accordingly, the density of steel is 8030 *kg/m^3*, and the density of glass is 2250 *kg/m^3* [76].

The latent coefficients for glass and steel are 15.9 *MJ/kg* and 32.9 *MJ/kg* respectively; the thickness of the reflector is 1*mm* [77].

Table 4 shows the SO_x, NO_x and CO_2 emission values for different base fluids and nanofluids studied in a parabolic collector with a smooth tube. The amount of environmental pollutants, created for the collector's operation with nanofluid, is less than the base fluid. As shown in Table 4, the lowest pollutant content is related to the *Water-SWCNT-CuO* hybrid nanofluid.

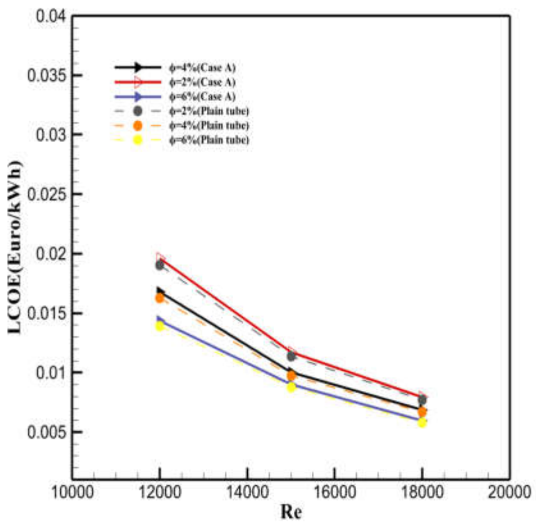

Fig. 28: Reynolds-*LCOE* variations for sample A and sample tube

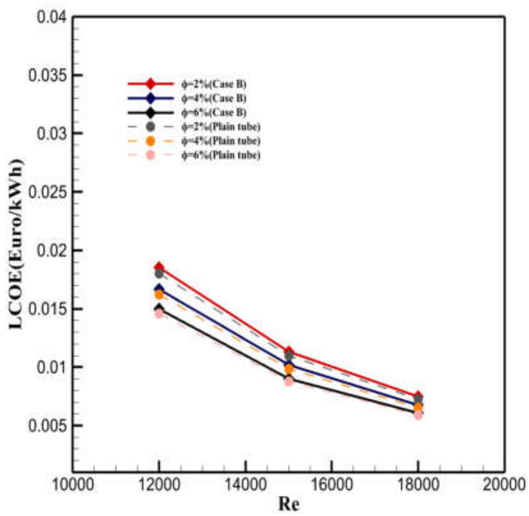

Fig. 29: Reynolds-*LCOE* variations for sample B and sample tube sample tube

The number of environmental pollutants in the collector life cycle increases when a hybrid turbulator is used instead of a smooth tube in the absorbent tube; also, the number of environmental pollutants in the collector life cycle increases as shown in Table5. An increase in environmental pollutants occurs by using an absorbent tube with hybrid turbulator in comparison with a smooth adsorbent for fluid of various factors including *Water, Water-CuO, Water-SWCNT, Water-SWCNT-CuO*, 9.05%, 9.08%, 9.08%, and 9.09% respectively. On the other hand, as shown in Tables 4 and 5, the lowest environmental pollutants occur when the operating fluid is a *Water-SWCNT-CuO*. Table 5 shows the values of *PTC* environmental pollutants for absorbent tubes with a hybrid turbulator for different operating fluids.

Table 4: Values of PTC environmental pollutants with a smooth adsorbent tube for different operating fluids

	Water	*Water-CuO*	*Water-SWCNT*	*Water-SWCNT-CuO*
Latent energy	13670.12	13665.87	13667.24	13665.21
CO_2	8340.13	8337.34	8338.10	8337.02
SO_x	4.3523	4.3508	4.3511	4.3506
NO_x	7.3147	7.3126	7.3131	7.3123

Table 5: Values of PTC environmental pollutants for absorbent tubes with a hybrid turbulator for different operating fluids

	Water	*Water-CuO*	*Water-SWCNT*	*Water-SWCNT-CuO*
Latent energy	14770.2	14768.3	14769	14768.2
CO_2	9094.9	9094.4	9095.2	9094.4
SO_x	4.75	4.75	4.75	4.75
NO_x	7.98	7.98	7.98	7.98

Environmental calculations based on the latent energy method, presented above, are only related to the collector construction stage. Other life cycle stages are ignored. Given that an amount of carbon dioxide obtained during the *PTC* fabrication phase due to latent energy, if the amount of carbon dioxide emissions during the collector life cycle is calculated, the amount of CO_2 emissions at other stages will estimated. To calculate the CO_2 emission in the collector life cycle, the following method can be used [78]:

$$x_{CO_2} = y_{CO_2} E_s t_{working} \tag{40}$$

Where x_{CO2} is carbon dioxide emission (*kg/day*), y_{CO2} is estimated CO_2 emission for solar collectors (*kg/W.h*), and working is the number of working hours of the collector per day. The following assumptions are made to estimate the amount of carbon dioxide emissions during the collector's life cycle. For a 25-year life span of *PTC* [79], with the number of sunny days at 300 [80, 81], the number of working hours per day of the collector at 7 hours, and the average amount of incident radiation 650 (W/m^2) are assumed. Also, the estimated CO_2 emission for solar collectors is 0.000013 (*kg/W.h*) [82]. Thus, it is observed that about 70 to 80% of the emissions are related to the *PTC* manufacturing phase, and about 20 to 30% of the emissions are related to other stages of the life cycle including distribution, maintenance, and disposal.

Due to the low production of environmental pollutants in the distribution, maintenance, and disposal of the life cycle of solar collectors, most environmental calculations are performed only based on the manufacturing phase regardless of other steps [82, 83]. The amount of useful heat obtained using *PTC* can be calculated with maximum thermal efficiency. If this amount of heat were obtained using fossil fuels, it would create a lot of environmental pollutants. For this purpose, three fossil fuels, natural gases, coal, and diesel are used to calculate the amount of carbon dioxide. CO_2 emissions for different fossil fuels are determined based on standard emission factors.

9. Conclusion

The numerical study of three-dimensional circular tubes integrated with two types of twisted-tape turbulators and two different scales was conducted. The range of volume fractions of nanoparticles between 2-6% with a range of Reynolds numbers from 12000-18000 was comprehensively investigated. Computational results showed that scale 1 (Sample A) increased heat transfer and collector efficiency, especially at high Reynolds numbers.

- Nanoparticle concentration and Reynolds number increase Nu_{avg}, coefficient of friction, and *PEC*. For example, the *PEC* value in the Reynolds number, 12000, increases by about 1.67% as the nanofluid concentration increases from 2 to 6%.
- The efficiency of the solar collector was reduced when the scale of the twisted-tape turbulator was reduced to (sample B). The highest value of η for sample A was obtained in Reynolds number 12000 and ϕ = 2% with the value of 0.55.
- The highest PEC value (1.21) was obtained at *Re* = 12000 and ϕ = 2%, and the lowest PEC value (0.93) was obtained at *Re* = 18000 and ϕ = 2% for the tube with sample A turbulator (scale 1).
- The Nu_{ave} in a tube with a combined turbulator (sample B) was about 15% higher than a tube with a TT (sample A)
- The use of a turbulator in the form of a twisted strip and a combination with a coil increased the HT rate.
- In the present study, using a larger scale (sample A) compared with sample B, increased the efficiency of the solar collector at a high Reynolds number.
- The amount of environmental pollutants created for the operation of the collector with two-phase HNF was less than the base fluid.

Nomenclature

C_p	specific heat ($kJ/kg.K$)
D	Diameter of the tube (mm)
h	heat transfer coefficient ($W/m2.k$)
k	thermal conductivity
Nu	Nusselt number
P	Pressure (*Pa*)
Pr	Prandtl number
Re	Reynolds number
q"	Heat flux (W/m^2)
T	Temperature (K)
TT	twisted tape
NP	Nanoparticle
NF	Nanofluid
HNF	Hybrid NanoFluid
PEC	performance evaluation criterion
FSP	field synergy principle
Greek symbol	
α	thermal diffusivity (m^2/s)
μ	dynamic viscosity ($kg/m.s$)
K	turbulent kinetic energy(m^2/s^2)
ρ	density (kg/m^3)
τ	wall shear stress (N/m^2)
ϕ	Nanoparticles Volume Fraction
η	Solar collector efficiency
ε	exergy efficiency
Subscripts	
i,j	tensor notations
x,y,z	Cartesian coordinates
avg	average
eff	effective property
in	inlet
out	outlet
p	partical
s	solid

References

[1] Borunda, M., R. Garduno-Ramirez, and O. Jaramillo, "*Optimal operation of a parabolic solar collector with twisted-tape insert by multi-objective genetic algorithms*", Renewable Energy, 143: p. 540-550, 2019., doi:10.1016/j.renene.2019.05.030

[2] Duan, Z., Yin, Q., Li, C., Dong, L., Bai, Y., Zhang, Y., "*Milling force and surface morphology of 45 steel under different Al2O3 nanofluid concentrations*", The

International Journal of Advanced Manufacturing Technology, Vol. 107, pp. 1277-1296, 2020., doi:10.1007/s00170-020-04969-9

[3] Kumar, R. and P. Chand, "*Performance prediction of extended surface absorber solar air collector with twisted tape inserts*", Solar Energy, Vol. 169: pp. 40-48, 2018., doi:10.1016/j.solener.2018.04.021

[4] Liu, X., Rao, R., Shi, J., He, J., Zhao, Y., Liu, J., Du, H., "*Effect of oxygen vacancy and A-site-deficiency on the dielectric performance of BNT-BT-BST relaxors*", Journal of Alloys and Compounds, Vol. 875, pp. 159999, 2021., doi:10.1016/j.jallcom.2021.159999

[5] Borunda, M., Jaramillo, O.A., Dorantes, R., Reyes, A., "*Organic Rankine Cycle coupling with a Parabolic Trough Solar Power Plant for cogeneration and industrial processes*", Renewable Energy, Vol. 86, pp. 651-663, 2016., doi:10.1016/j.renene.2015.08.041

[6] Sallaberry, F., Pujol-Nadal, R., Garcia de Jalón, A., Martínez-Moll, V., "*Towards a Standard Testing Methodology for Medium-temperature Solar Collectors with Variable Geometry*", Energy Procedia, Vol. 57, pp. 2904-2913, 2014., doi:10.1016/j.egypro.2014.10.325

[7] Kumar, C.N., Murugesan, P., "*Review on twisted tapes heat transfer enhancement*", International Journal of Scientific and Engineerin`g Research, Vol. 3, pp. 1-9, 2012., doi:10.1016/j.rser.2016.04.051

[8] Abed, A.M., Alghoul, M.A., Sopian, K., Mohammed, H.A., Majdi, H.SH., Al-Shamani, A.N., "*Design characteristics of corrugated trapezoidal plate heat exchangers using nanofluids*", Chemical Engineering and Processing: Process Intensification, Vol. 87, pp. 88-103, 2015., doi:10.1016/j.cep.2014.11.005

[9] Ajeel, R.K., Salim, V.S.L., Sopian, K., Yusoff, M.Z.,Hasnan, KH., Ibrahim, A., Al-Waeli, A., "*Turbulent convective heat transfer of silica oxide nanofluid through corrugated channels: An experimental and numerical study*", International Journal of Heat and Mass Transfer, Vol. 145, pp. 118806, 2019., doi:10.1016/j.ijheatmasstransfer.2019.118806

[10] Bisht, V.S., Patil, A.K., Gupta, A., "*Review and performance evaluation of roughened solar air heaters*", Renewable and Sustainable Energy Reviews, Vol. 81,pp. 954-97, 2018., doi:10.1016/j.rser.2017.08.036

[11] Kumar, A., Kim, M.-H., "*Convective heat transfer enhancement in solar air channels*", Applied Thermal Engineering, Vol. 89, pp. 239-261, 2015., doi:10.1016/j.applthermaleng.2015.06.015

[12] Kareem, Z.S., Mohd Jaafar, M.N., Lazim, T.M., Abdullah, SH., Abdulwahid, A.F., "Passive heat transfer enhancement review in corrugation", Experimental Thermal and Fluid Science, Vol. 68: pp. 22-38, 2015, doi:10.1016/j.expthermflusci.2015.04.012.

[13] Navickaitė, K., Cattani, L., Bahl, C.R.H., Engelbrecht, K., "*Elliptical double corrugated tubes for enhanced heat transfer*", International Journal of Heat and Mass Transfer, Vol. 128, pp. 363-377, 2019., doi:10.1016/j.ijheatmasstransfer.2018.09.003

[14] Hussein, A.M., Sharma, K.V., Bakar, R.A., Kadirgama, K., A., "R*eview of forced convection heat transfer enhancement and hydrodynamic characteristics of a nanofluid*", Renewable and Sustainable Energy Reviews, Vol. 29, pp. 734-743, 2014., doi:10.1016/j.rser.2013.08.014

[15] Khoshvaght-Aliabadi, M., Eskandari, M., "*Influence of twist length variations on thermal–hydraulic specifications of twisted-tape inserts in presence of Cu–water nanofluid*", Experimental Thermal and Fluid Science, Vol. 61, pp. 230-240, 2015., doi:10.1016/j.expthermflusci.2014.11.004

[16] Pang, C., Lee, J.W., Kang, Y.T., "*Review on combined heat and mass transfer characteristics in nanofluids*", International Journal of Thermal Sciences, Vol. 87, pp. 49-67, 2015., doi:10.1016/j.ijthermalsci.2014.07.017

[17] Gao, T., Zhang, X., Li, CH., Zhang, Y., Yang, M., Jia, D., Ji, H., Zhao, Y., Li, R., Yao, P., Zhu, L., "*Surface morphology evaluation of multi-angle 2D ultrasonic vibration integrated with nanofluid minimum quantity lubrication grinding*", Journal of manufacturing processes, Vol. 51, pp. 44-61, 2020., doi:10.1016/j.jmapro.2020.01.024

[18] Jaisankar, S., Radhakrishnan, T.,Sheeba, K., "*Experimental studies on heat transfer and friction factor characteristics of forced circulation solar water heater system fitted with helical twisted tapes*", Solar Energy, Vol. 83, pp. 1943-1952, 2009., doi:10.1016/j.solener.2009.07.006

[19] Sui, M., Li, C., Wu, W., Yang, M., Muhammad Ali, H., Zhang, Y., Jia, D., Hou, Y., "*Temperature of grinding carbide with castor oil-based MoS2 nanofluid minimum quantity lubrication*", Journal of Thermal Science and Engineering Applications, Vol. 13,pp.14-25, 2021., doi:10.1115/1.4049982

[20] Bellos, E.,Tzivanidis, C., "*Enhancing the performance of evacuated and non-evacuated parabolic trough collectors using twisted tape inserts, perforated plate inserts and internally finned absorber*", Energies, Vol. 11, pp. 1129. 2018., doi:10.3390/en11051129

[21] Jafar, K.S.,Sivaraman, B., "*Performance characteristics of parabolic solar collector water heater system fitted with nail twisted tapes absorber*", J. Eng. Sci. Technol, Vol. 12, pp. 608-621. 2017., doi:10.1016/j.rser.2018.04.093

[22] Nakhchi, M., Rahmati, M., "*Entropy generation of turbulent Cu–water nanofluid flows inside thermal systems equipped with transverse-cut twisted turbulators*", Journal of Thermal Analysis and Calorimetry, Vol. 143, pp. 2475-2484, 2021., doi:10.1007/s10973-020-09960-w

[23] ErfanianNakhchi, M. Rahmati, M., "*Turbulent flows inside pipes equipped with novel perforated V-shaped rectangular winglet turbulators: numerical simulations*", Journal of Energy Resources Technology, Vol. 142, pp. 123-135, 2020., doi:10.1115/1.4047319

[24] Jaramillo, O.A., Borunda, M., Velazquez-Lucho, K.M., Robles, M., "*Parabolic trough solar collector for low enthalpy processes: An analysis of the efficiency enhancement by using twisted tape inserts*", Renewable energy, Vol. 93, pp. 125-141, 2016., doi:10.1016/j.renene.2016.02.046

[25] Wang, M., Yang, L., Hu, B., Liu, J., He, L., Jia, Q., Song, Y., Zhang, Z., "*Bimetallic NiFe oxide structures derived from hollow NiFe Prussian blue nanobox for label-free electrochemical biosensing adenosine triphosphate*", Biosensors and Bioelectronics, Vol. 113, pp. 16-24, 2018., doi:10.1016/j.bios.2018.04.050

[26] Smithberg, E., Landis, F., "*Friction and forced convection heat-transfer characteristics in tubes with twisted tape swirl generators*", Vol. 86, pp. 39-48, 1964., doi:10.1115/1.3687061

[27] Hong, S.,Bergles, A., "*Augmentation of laminar flow heat transfer in tubes by means of twisted-tape inserts*", Vol. 98, pp. 251-256, 1976., doi:10.1115/1.3450527

[28] Manglik, R.M., Bergles, A.E., "*Heat transfer and pressure drop correlations for twisted-tape inserts in isothermal tubes: Part II—Transition and turbulent flows*", Vol. 115, pp. 890-896, 1993., doi:10.1115/1.2911384

[29] Klepper, O., "*HEAT TRANSFER PERFORMANCE OF SHORT TWISTED TAPES*", Oak Ridge National Lab., Tenn, 1972., doi:10.2172/4645882

[30] Dasmahapatra, J. M., Rao, R., "*Laminar flow heat transfer to generalized power law fluids inside circular tubes fitted with regularly spaced twisted tape elements for uniform wall temperature condition*", Heat Transfer Division HTD,. Vol. 174,pp. 51-58, 1991., doi:10.1016/j.renene.2016.02.046

[31] Date, A., Gaitonde, U., "*Development of correlations for predicting characteristics of laminar flow in a tube fitted with regularly spaced twisted-tape elements*", Experimental Thermal and Fluid Science, Vol. 3,pp. 373-382, 1990., doi:10.1016/0894-1777(90)90035-6

[32] Date, A.,Singham, J., "*Numerical prediction of friction and heat transfer characteristics of fully developed laminar flow in tube containing twisted tapes tapes in Mechanical Engineering*", ASME-AMER SOC MECHANICAL ENG 345 E 47TH ST, Newyork, NY 10017.1972., doi:10.1016/0142-727X(90)90058-J

[33] Date, A.W., "*Prediction of fully-developed flow in a tube containing a twisted-tape*", International journal of heat and mass transfer, Vol. 17,pp. 845-859, 1974., doi:10.1016/0017-9310(74)90152-5

[34] Eiamsa-Ard, S., Promvonge, P., "*Thermal characteristics in round tube fitted with serrated twisted tape*", Applied Thermal Engineering, Vol. 30, pp. 1673-1682, 2010., doi:10.1016/j.applthermaleng.2010.03.026

[35] Piriyarungrod, N., Kumar,M., Thianpong, C., Pimsarn, M., Chuwattanakul, V., Eiamsa-ard, S., "*Intensification of thermo-hydraulic performance in heat exchanger tube inserted with multiple twisted-tapes*", Applied Thermal Engineering, 136: p. 516-530, 2018., doi:10.1016/j.applthermaleng.2018.02.097

[36] Abed, A.M., Majdi, H. SH., Hussein, Z., Fadhil, D., Abdulkadhim, A., "*Numerical analysis of flow and heat transfer enhancement in a horizontal pipe with P-TT and V-Cut twisted tape*", Case studies in thermal engineering, Vol. 12, pp. 749-758, 2018., doi:10.1016/j.csite.2018.10.004

[37] Saravanan, A., Senthilkumaar, J., Jaisankar, S., "*Performance assessment in V-trough solar water heater fitted with square and V-cut twisted tape inserts*", Applied Thermal Engineering, Vol. 102, pp. 476-486, 2016., doi:10.1016/j.applthermaleng.2016.03.088

[38] Zhang, S., Lu, L., Dong, CH., Hyun Cha, S., "*Performance evaluation of a double-pipe heat exchanger fitted with self-rotating twisted tapes*", Applied Thermal Engineering, Vol. 158,pp. 113770, 2019., doi:10.1016/j.applthermaleng.2019.113770

[39] Peyghambarzadeh, S., Hashemabadi, S.H., Hoseini, S.M., SeifiJamnani, M., "Experimental study of heat transfer enhancement using water/ethylene glycol based nanofluids as a new coolant for car radiators", International communications in heat and mass transfer, Vol. 38, pp. 1283-1290, 2011., doi:10.1016/j.icheatmasstransfer.2011.07.001

[40] Rebsdat, S., Mayer, D., "*Ethylene glycol. Ullmann's Encyclopedia of Industrial Chemistry*", Vol. 495, pp. 1453-1495, 2000, doi:10.1002/14356007.a10_101

[41] Olia, H., Torabi, M., Bahiraei, M., Ahmadi, M.H., Goodarzi, M., Safaei, M.R., "*Application of nanofluids in thermal performance enhancement of parabolic trough solar collector: state-of-the-art*", Applied Sciences, Vol. 9, pp. 463. 2019., doi:10.3390/app9030463

[42] Korres, D., Bellos, E., Tzivanidis, C., "*Investigation of a nanofluid-based compound parabolic trough solar collector under laminar flow conditions*", Applied Thermal Engineering, Vol. 149, pp. 366-376, 2019.,

doi:10.1016/j.applthermaleng.2018.12.077

[43] Li, Z., Sheikholeslami, M., Jafaryar, M., Shafee, A.,Chamkha, A.J., "*Investigation of nanofluid entropy generation in a heat exchanger with helical twisted tapes*", Journal of Molecular Liquids, Vol. 266,pp. 797-805, 2018., doi:10.1016/j.molliq.2018.07.009

[44] Gnanavel, C., Saravanan, R., Chandrasekaran, M., "Heat transfer enhancement through nano-fluids and twisted tape insert with rectangular cut on its rib in a double pipe heat exchanger" Materials Today, Proceedings, Vol. 21, pp. 865-869, 2020., doi:10.1016/j.matpr.2019.07.606

[45] Faris Abdullah, M., Zulkifli, R., Harun, Z., Abdullah, SH., Wan Ghopa, W.A., Soheil Najm, A., Sulaiman, N.H., "Impact of the TiO_2 nanosolution concentration on heat transfer enhancement of the twin impingement jet of a heated aluminum plate", Micromachines, Vol. 10,pp. 176-210, 2019., doi:10.3390/mi10030176

[46] Akyürek, E.F., Geliş, K., Şahin, B., Manay, E., "*Experimental analysis for heat transfer of nanofluid with wire coil turbulators in a concentric tube heat exchanger*", Results in Physics, Vol. 9,pp. 376-389, 2018., doi:10.1016/j.rinp.2018.02.067

[47] Arani, A.A.A., Sadripour, S., Kermani, S., "Nanoparticle shape effects on thermal-hydraulic performance of boehmite alumina nanofluids in a sinusoidal–wavy mini-channel with phase shift and variable wavelength", International Journal of Mechanical Sciences, Vol. 128, pp. 550-563, 2017., doi:10.1016/j.ijmecsci.2017.05.030

[48] Dezfulizadeh, A., Aghaei, A., HassaniJoshaghani, A., Najafizadeh, M.M., "An experimental study on dynamic viscosity and thermal conductivity of water-Cu-SiO_2-MWCNT ternary hybrid nanofluid and the development of practical correlations", Powder Technology, Vol. 389, pp. 215-234, 2021., doi:10.1016/j.powtec.2021.05.029

[49] Soltani, O., Akbari, M., "Effects of temperature and particles concentration on the dynamic viscosity of MgO-MWCNT/ethylene glycol hybrid nanofluid: experimental study", Physica E: Low-dimensional Systems and Nanostructures, Vol. 84,pp. 564-570, 2016., doi:10.1016/j.physe.2016.06.015

[50] Ahmad, S., Ashraf, M., Ali, K., "*Numerical simulation of viscous dissipation in a micropolar fluid flow through a porous medium*", Journal of Applied Mechanics and Technical Physics, Vol. 60, pp. 996-1004, 2019., doi:10.1134/S0021894419060038

[51] Ahmad, S., Ashraf M., Ali, K., "Nanofluid flow comprising gyrotactic microorganisms through a porous medium. Journal of Applied Fluid Mechanics", Vol. 13, pp. 1539-1549, 2020., doi: 10.36884/jafm.13.05.31030

[52] Ahmad, S., Ashraf, M., Ali, K., "*Bioconvection due to gyrotactic microbes in a nanofluid flow through a porous medium. Heliyon*", Vol. 6, pp. 105832, 2020., doi:10.1016/j.heliyon.2020.e05832

[53] Ahmad, S., Ashraf, M., Ali, K., "*Simulation of thermal radiation in a micropolar fluid flow through a porous medium between channel walls*", Journal of Thermal Analysis and Calorimetry, Vol. 144, pp. 941-953, 2021., doi:10.1007/s10973-020-09542-w

[54] Duangthongsuk, W.,Wongwises, S., "An experimental study on the heat transfer performance and pressure drop of TiO_2-water nanofluids flowing under a turbulent flow regime", International Journal of Heat and Mass Transfer,Vol. 53, pp. 334-344, 2010., doi:10.1016/j.ijheatmasstransfer.2009.09.024

[55] Dezfulizadeh, A., Aghaei, A., HassaniJoshaghani, A., Najafizadeh, M.M.,"Exergy efficiency of a novel heat exchanger under MHD effects filled with water-based Cu–SiO_2-MWCNT ternary hybrid nanofluid based on empirical data. Journal of Thermal Analysis and Calorimetry", Vol. 147, pp. 4781-4804, 2022., doi:10.1007/s10973-021-10867-3

[56] Roohbakhsh Meyary Dovom, A., Aghaei, A., Hassani Joshaghani, A., Dezfulizadeh, A., Azadi kakavandi, A., "Numerical analysis of heating aerosol carbon nanofluid flow in a power plant recupesrator with considering ash fouling: a deep learning approach", Engineering Analysis with Boundary Elements, Vol. 141, pp. 75-90, 2022., doi:10.1016/j.enganabound.2022.05.001

[57] Aghaei, A., Enayati, M., Beigi, N., Ahmadi, A., Pourmohamadian, H., Sadeghi, SH., Dezfulizadeh, A., Golzar, A.,"Comparison of the effect of using helical strips and fines on the efficiency and thermal–hydraulic performance of parabolic solar collectors", Sustainable Energy Technologies and Assessments, Vol. 52,pp. 102254, 2022., doi:10.1016/j.seta.2022.102254

[58] Rostami, S., Sepehrirad, M., Dezfulizadeh, A., Kadhim Hussein, A., ShahsavarGoldanlou, A., SafdariShadloo, M.,"Exergy optimization of a solar collector in flat plate shape equipped with elliptical pipes filled with turbulent nanofluid flow: a study for thermal management", Water,Vol. 12, pp. 2294, 2020., doi:10.3390/w12082294

[59] Versteeg, H.K., Malalasekera, W., "*An introduction to computational fluid dynamics: the finite volume method*", Pearson education, 2007.

[60] Shakiba, A., Vahedi, K., "Numerical analysis of magnetic field effects on hydro-thermal behavior of a magnetic nanofluid in a double pipe heat exchanger", Journal of Magnetism and Magnetic Materials, Vol. 402,pp. 131-142, 2016., doi:10.1016/j.jmmm.2015.11.039

[61] Nazir, M.S., Ghasemi, A., Dezfulizadeh, A., Abdalla, A.N., "*Numerical simulation of the performance of a novel parabolic solar receiver filled with nanofluid*",

Journal of Thermal Analysis and Calorimetry, Vol. 144, pp. 2653-2664. 2021., doi:10.1007/s10973-021-10613-9

[62] ShahsavarGoldanlou, Sepehrirad, M., Dezfulizadeh, A., Golzar, A., Badri, M., Rostami, S., "*Effects of using ferromagnetic hybrid nanofluid in an evacuated sweep-shape solar receiver*", Journal of Thermal Analysis and Calorimetry, Vol. 143,pp. 1623-1636, 2021., doi:10.1007/s10973-020-09903-5

[63] Hasanpour, A., Farhad,i M., Sedighi, K., "*Intensification of heat exchangers performance by modified and optimized twisted tapes*", Chemical Engineering and Processing-Process Intensification, Vol. 120, pp. 276-285, 2017., doi:10.1016/j.cep.2017.07.026

[64] Rashidi, S., Akbarzadeh, A., Karimi, N., Masoodi, R., "Combined effects of nanofluid and transverse twisted-baffles on the flow structures, heat transfer and irreversibilities inside a square duct–a numerical study", Applied Thermal Engineering, Vol. 130, pp. 135-148. 2018., doi:10.1016/j.applthermaleng.2017.11.048

[65] Menter, F., Esch, T., Kubacki, S., "*Transition modelling based on local variables, Engineering Turbulence Modelling and Experiments*", Vol. 5, pp. 555-564. 2002., doi:10.1016/B978-008044114-6/50053-3

[66] Incropera, F., "*Fundamentals of Heat and Mass Transfer 6th Edition*", Fundamentals of Heat and Mass Transfer. 2007.

[67] Petela, R., "*Exergy of undiluted thermal radiation*", Solar energy,Vol. 74, pp. 469-488, 2003., doi:10.1016/S0038-092X(03)00226-3

[68] Candau, Y., "*On the exergy of radiation*", Solar Energy, Vol. 75,pp. 241-247, 2003., doi:10.1016/j.solener.2003.07.012

[69] Kasaiean, A., Sameti, M., Daneshazarian, R., Noori, Z., Adamian, A., Ming, T., "*Heat transfer network for a parabolic trough collector as a heat collecting element using nanofluid*", Renewable energy, Vol. 123,pp. 439-449, 2018., doi:10.1016/j.renene.2018.02.062

[70] Zare, V., Moalemian, A., "Parabolic trough solar collectors integrated with a Kalina cycle for high temperature applications: Energy, exergy and economic analyses", Energy Conversion and Management, Vol. 151: pp. 681-692, 2017., doi:10.1016/j.enconman.2017.09.028

[71] Malekan, M., Khosravi, A., Syri, S., "Heat transfer modeling of a parabolic trough solar collector with working fluid of Fe3O4 and CuO/Therminol 66 nanofluids under magnetic field", Applied Thermal Engineering, Vol. 163,pp. 114435, 2019., doi:10.1016/j.applthermaleng.2019.114435

[72] Bellos, E., Tzivanidis, C., Daniil, I., "*Thermal and exergetic evaluation of parabolic trough collectors with finned absorbers operating with air*", Proceedings of the Institution of Mechanical Engineers, Part A: Journal of Power and Energy, Vol. 231, pp. 631-644, 2017., doi:10.1177/0957650917712403

[73] Faizal, M., Saidur, R., Mekhilef, S., Alim, M.A., "*Energy, economic and environmental analysis of metal oxides nanofluid for flat-plate solar collector*", Energy Conversion and Management, Vol. 76,pp. 162-168, 2013., doi:10.1016/j.enconman.2013.07.038

[74] Faizal, M., Saidur, R., Mekhilef, S., Hepbasli, A., Mahbubul, I.M., "*Energy, economic, and environmental analysis of a flat-plate solar collector operated with SiO_2 nanofluid*", Clean Technologies and Environmental Policy,Vol. 17, pp. 1457-1473,2015., doi:10.1007/s10098-014-0870-0

[75] Michael Joseph Stalin, P., Arjunan, T.V., Matheswaran, M.M., Dolli, H., Sadanandam, N., "*Energy, economic and environmental investigation of a flat plate solar collector with CeO_2/water nanofluid*", Journal of Thermal Analysis and Calorimetry, Vol. 139, pp. 3219-3233.2020., doi:10.1007/s10973-019-08670-2

[76] Moosavian, S.F., Borzuei,D., Ahmadi,A., "Energy, exergy, environmental and economic analysis of the parabolic solar collector with life cycle assessment for different climate conditions", Renewable Energy, Vol. 165,pp. 301-320, 2021., doi:10.1016/j.renene.2020.11.036

[77] Mashhadian, A., Heyhat,M.M., Mahian,O., "*Improving environmental performance of a direct absorption parabolic trough collector by using hybrid nanofluids*", Energy Conversion and Management, Vol. 244, pp. 114450.2021., doi:10.1016/j.enconman.2021.114450

[78] Lei, D., Fu, X., Ren, Y., Yao, F., Wang, Z., "*Temperature and thermal stress analysis of parabolic trough receivers*", Renewable Energy, Vol. 136, pp. 403-413,2019., doi:10.1016/j.renene.2019.01.021

[79] Baird, G., Alcorn,A., Haslam,P., "*The energy embodied in building materials-updated New Zealand coefficients and their significance*", Transactions of the Institution of Professional Engineers New Zealand: Civil Engineering Section, Vol. 24, pp. 46-54, 1997.

[80] Caliskan, H., "Energy, exergy, environmental, enviroeconomic, exergoenvironmental (EXEN) and exergoenviroeconomic (EXENEC) analyses of solar collectors", Renewable and Sustainable Energy Reviews, Vol. 69,pp. 488-492, 2017., doi:10.1016/j.rser.2016.11.203

[81] Dieckmann, S., Dersch, J., Giuliano, S., Puppe, M., Lüpfert, E., Hennecke, K., Pitz-Paal, R., Taylor, M., Ralon, P., "*LCOE reduction potential of parabolic trough and solar tower CSP technology until 2025. in AIP Conference Proceedings*", AIP Publishing LLC, Vol. 850, pp. 160-193, 2017., doi:10.1063/1.4984538

[82] Najafi, G., Ghobadian, B., Mamat, R.,Yusaf, T., Azmi, W.H., "*Solar energy in Iran: Current state and outlook*", Renewable and Sustainable Energy Reviews, Vol. 49,pp. 931-942,2015., doi:10.1016/j.rser.2015.04.056

[83] Aghaei, A., Dezfulizadeh A., Fadaeidehar, A., Sepehrirad, M., Mazaheri, H., "Determination of Energy Efficiency and Exergy of Solar Collector Bed, Operating Plate under Turbulent Nanoscale Flow with Molybdenum Disulfide Nanoparticles in Different Morphologies for Tropical Regions of Iran", Energy Engineering & Management, Vol. 12, pp. 130-143, 2022., (In Persion) doi: 10.22052/12.1.130